Journal of Fluids and Structures 27 (2011) 1086–1096

Contents lists available at ScienceDirect

Journal of Fluids and Structures

journal homepage: www.elsevier.com/locate/jfs

Flutter instability of a fluid-conveying fluid-immersed pipe affixed to a rigid body

Aren Hellum [a], Ranjan Mukherjee [a,*], Andrew J. Hull [b]

[a] Department of Mechanical Engineering, 2555 Engineering Building, Michigan State University, East Lansing, MI 48824-1226, United States
[b] Advanced Acoustic Systems Division, Autonomous and Defensive Systems Department, Naval Undersea Warfare Center, Newport, RI 02841, United States

ARTICLE INFO

Article history:
Received 28 June 2010
Accepted 11 March 2011
Available online 6 April 2011

Keywords:
Fluid-conveying pipe
Fluid-immersed pipe
External flow
Flutter instability
Boundary conditions
Submersible
Jet propulsion
Fish propulsion
Thrust
Efficiency

ABSTRACT

A set of simplified boundary conditions for a flexible beam connected to a rigid body at one end and free at the other end is presented and applied to the case of a fluid-conveying, fluid-immersed pipe. These boundary conditions represent an analytically tractable approximation to those of a submersible which uses a combination of jet action and flutter instability induced tail motion to produce thrust. The boundary conditions are made non-dimensional, and the effect of the non-dimensional mass of the rigid body on system stability is assessed. The neutral stability of this system is determined within a two-parameter space consisting of the velocity of the fluid within the tail, and the forward speed of the submersible. Equations in the literature, derived using slender-body theory, were used to compute the sign of the thrust produced by the tail and the tail's Froude efficiency for the neutrally stable waveforms of the beam.

1. Introduction

The dynamics of fluid-conveying pipes have been well-examined in the literature, both with external flow (Hannoyer and Païdoussis, 1978; Païdoussis, 2004) and without external flow (Païdoussis, 1998). Many boundary conditions have also been studied. The cantilever (Bourrières, 1939; Gregory and Païdoussis, 1966) and pinned–pinned (Ashley and Haviland, 1950) conditions form the bulk of the early entries in the literature, and somewhat more exotic conditions, such as that of a clamped foundation with a spring support (Chen, 1971) have since been added. It is notable that the boundary conditions considered tend to be those found in classical engineering practice, or improvements upon them. This is in contrast to the "theory first" bent of mind expressed in the literature (Païdoussis and Li, 1993, for example), in which theoretical developments precede practical applications. In this paper, the boundary conditions of a fluid-conveying fluid-immersed pipe, affixed at one end to a rigid body and free at the other end, are developed and the resultant dynamics of the pipe is discussed. Far from being a purely theoretical exercise, this work has been aimed at analyzing a novel type of submersible.

In the 1970s, Païdoussis and coworkers built and tested (Païdoussis, 1976) a propulsor which exploited the dynamics of a fluid-conveying pipe. The superficial similarity between a fluttering fluid-conveying cantilever and a fish is compelling; both motions are that of a traveling wave which grows from tip to tail, and it is easy to appreciate that the well-documented efficiency of fish-like motion (Gray, 1936; Lighthill, 1970) was the motivation for this type of

* Corresponding author. Tel.: +1 517 355 1834; fax: +1 517 353 1750.
E-mail addresses: hellumar@egr.msu.edu (A. Hellum), mukherji@egr.msu.edu (R. Mukherjee), andrew.hull@navy.mil (A.J. Hull).

0889-9746/$ - see front matter © 2011 Elsevier Ltd. All rights reserved.
doi:10.1016/j.jfluidstructs.2011.03.002

Report Documentation Page

Form Approved
OMB No. 0704-0188

1. REPORT DATE	2. REPORT TYPE	3. DATES COVERED
2011		**00-00-2011 to 00-00-2011**

4. TITLE AND SUBTITLE	5a. CONTRACT NUMBER
Flutter Instability Of A Fluid-Conveying Fluid-Immersed Pipe Affixed To A Rigid Body	5b. GRANT NUMBER
	5c. PROGRAM ELEMENT NUMBER
6. AUTHOR(S)	5d. PROJECT NUMBER
	5e. TASK NUMBER
	5f. WORK UNIT NUMBER
7. PERFORMING ORGANIZATION NAME(S) AND ADDRESS(ES) **Michigan State University,Department of Mechanical Engineering,2555 Engineering Building,East Lansing,MI,48824**	8. PERFORMING ORGANIZATION REPORT NUMBER
9. SPONSORING/MONITORING AGENCY NAME(S) AND ADDRESS(ES)	10. SPONSOR/MONITOR'S ACRONYM(S)
	11. SPONSOR/MONITOR'S REPORT NUMBER(S)

12. DISTRIBUTION/AVAILABILITY STATEMENT
Approved for public release; distribution unlimited

13. SUPPLEMENTARY NOTES
Journal of Fluids and Structures 27 (2011) 1086-1096,Government or Federal Purpose Rights License

14. ABSTRACT

15. SUBJECT TERMS

16. SECURITY CLASSIFICATION OF:			17. LIMITATION OF ABSTRACT	18. NUMBER OF PAGES	19a. NAME OF RESPONSIBLE PERSON
a. REPORT **unclassified**	b. ABSTRACT **unclassified**	c. THIS PAGE **unclassified**	**Same as Report (SAR)**	**12**	

mechanism. Although the fluttering motion of the tail was found to be a net gain above the thrust provided by the jet exhausting into the water, the efficiency did not approach that of a propeller, and after a patent (Païdoussis, 1978), the idea appears to have been dropped. The two works which comprise the published literature on this type of combination propulsor are primarily experimental, and in the next section we discuss some basic theoretical considerations needed to compute the thrust and efficiency in its motion.

We believe that several interim developments since Païdoussis' (1976) initial efforts make the fluttering fluid-conveying tail a compelling problem for reexamination. In the intervening 30 years, both battery and motor technologies have improved to the point that the prime mover and power source can be packaged into the neutrally buoyant hull of a submersible; whereas the hull used by Païdoussis was large relative to the propulsor, to the point that the beam could be considered a cantilever. A significant reduction in the size of the hull allows the tail motion to affect those of the hull, and vice versa. Analysis of a vehicle with a smaller hull therefore requires that the dynamics of the hull be considered when analyzing the stability of the fluid-conveying tail. A smaller hull significantly reduces drag and may in the future allow a vehicle of this type to harness the impressive maneuverability of fish. While the present communication does not consider the additional dynamics present in an accelerating and turning vehicle,[1] the boundary conditions presented here are the closest linear approximation to those found in the proposed submersible.

This paper is organized as follows. Section 2 provides the background for the dynamic equations of fluid conveying, fluid-immersed pipes and the mechanics of slender-body swimming. Section 3 presents the rigid body boundary conditions, non-dimensionalizes them, and describes the analytical method used for solution. Section 4 investigates the flow requirements for controlled flutter and calculations of thrust and efficiency of the waveforms produced by the fluttering tail. Concluding remarks and directions for future research are provided in Section 5.

2. Background

2.1. Fluid-conveying pipes

The equations of motion and boundary conditions for a cantilever pipe conveying fluid with constant velocity U_i, immersed in an inviscid fluid flowing with constant velocity U_e, and ignoring gravitational, viscous, pressurization and tensile effects, are as follows (Païdoussis, 2004):

$$EI\frac{\partial^4 y}{\partial x^4}+(MU_i^2+M_eU_e^2)\frac{\partial^2 y}{\partial x^2}+2(MU_i+M_eU_e)\frac{\partial^2 y}{\partial x\partial t}+(m+M+M_e)\frac{\partial^2 y}{\partial t^2}=0,$$

$$y(0,t)=0,\quad \frac{\partial y}{\partial x}(0,t)=0,\quad \frac{\partial^2 y}{\partial x^2}(L,t)=0,\quad \frac{\partial^3 y}{\partial x^3}(L,t)=0, \tag{1}$$

where $y(x,t)$ is the displacement of the pipe, as shown in Fig. 1, E, I and L denote Young's modulus, area moment of inertia, and length of the pipe, respectively, and m, M and M_e represent the mass per unit length of the beam, the internal (conveyed) fluid, and the external fluid. The masses per unit length of the beam and internal fluid can be easily computed but the mass per unit length of the external fluid requires approximation. One method for computation of M_e is to use the added mass coefficient (Brennan, 1982). For thin cross-sections, such as that of a flat plate, the added mass is equal to the mass of water within the cylinder which circumscribes the plate cross-section. A "finned tube", well-suited to providing both a fluid conduit and a tail of adequate span, is depicted in Fig. 2 with the area responsible for the added external mass marked. Viscous terms characteristic of the external flow (Hannoyer and Païdoussis, 1978) and internal flow (Hellum et al., 2010b) are of course needed to compute the overall efficiency of the submersible, and affect beam stability as well. However, to benefit from Lighthill's (1960) prior work on thrust and efficiency of an oscillating slender body and to keep the analysis simple, we have chosen to neglect these effects.

Eq. (1) may be non-dimensionalized via the following change of variables:

$$X=\frac{x}{L},\quad Y=\frac{y}{L},\quad T=\frac{t}{L^2}\left(\frac{EI}{m+M+M_e}\right)^{1/2}. \tag{2}$$

If we define the non-dimensional velocities u_i and u_e and the mass fractions β_i and β_e as follows:

$$u_i=\left(\frac{M}{EI}\right)^{1/2}U_iL,\qquad \beta_i=\frac{M}{m+M+M_e},$$

$$u_e=\left(\frac{M_e}{EI}\right)^{1/2}U_eL,\quad \beta_e=\frac{M_e}{m+M+M_e},$$

[1] A recent conference paper (Hellum et al., 2010a) does include these terms and solves the equations of motion with a finite difference scheme. The results presented in the current work were used to reduce the number of lengthy iterations required to find a thrust-producing region of operation.

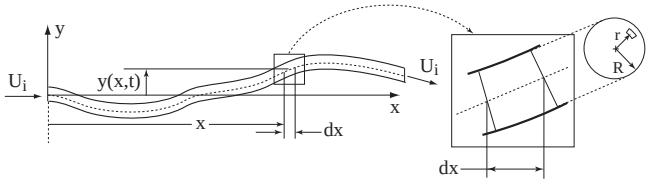

Fig. 1. A cantilevered fluid-conveying pipe, with a magnified view of a small length element.

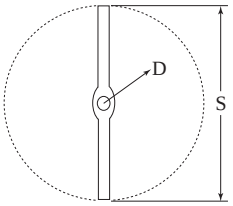

Fig. 2. The cross-section of a finned tube with fluid-conduit diameter D and tail span S. The dotted circle describes the area responsible for the added external mass M_e, which is equal to $0.25\rho_f\pi S^2$, where ρ_f is the density of the external fluid.

then Eq. (1) can be written in its non-dimensional form

$$\frac{\partial^4 Y}{\partial X^4}+(u_i^2+u_e^2)\frac{\partial^2 Y}{\partial X^2}+2(u_i\sqrt{\beta_i}+u_e\sqrt{\beta_e})\frac{\partial^2 Y}{\partial X\partial T}+\frac{\partial^2 Y}{\partial T^2}=0. \tag{3}$$

If we assume a separable form for $y(x,t)$ such that

$$y(x,t)=f(x)e^{i\Omega t},$$

the non-dimensional variable Y can then be written as

$$Y(X,T)=\phi(X)e^{i\omega t},\quad \omega=\left(\frac{m+M+M_e}{EI}\right)^{1/2}\Omega L^2. \tag{4}$$

Separation yields the ordinary differential equation and boundary conditions

$$\begin{aligned}&\frac{\partial^4\phi}{\partial X^4}+(u_i^2+u_e^2)\frac{\partial^2\phi}{\partial X^2}+2(u_i\sqrt{\beta_i}+u_e\sqrt{\beta_e})\,i\omega\frac{\partial\phi}{\partial X}-\omega^2\phi=0,\\ &\phi(0)=0,\quad \phi'(0)=0,\quad \phi''(1)=0,\quad \phi'''(1)=0,\end{aligned} \tag{5}$$

where ϕ', ϕ'', and ϕ''' denote the first, second, and third derivatives of ϕ with respect to X. The solution of ϕ is assumed to be of the form $\phi(X)=Ae^{zX}$. For specific values of u_i, u_e, β_i and β_e, the characteristic polynomial of Eq. (5) provides four roots z_n, where $z_n=z_n(\omega)$, $n=$ 1,2,3,4. The solution of $\phi(X)$ therefore takes the form

$$\phi(X)=A_1e^{z_1X}+A_2e^{z_2X}+A_3e^{z_3X}+A_4e^{z_4X}. \tag{6}$$

Substitution of Eq. (6) into Eq. (5) yields the identity

$$\underbrace{\begin{bmatrix}1 & 1 & 1 & 1\\ z_1 & z_2 & z_3 & z_4\\ z_1^2e^{z_1} & z_2^2e^{z_2} & z_3^2e^{z_3} & z_4^2e^{z_4}\\ z_1^3e^{z_1} & z_2^3e^{z_2} & z_3^3e^{z_3} & z_4^3e^{z_4}\end{bmatrix}}_{\mathbf{Z}}\begin{bmatrix}A_1\\A_2\\A_3\\A_4\end{bmatrix}=\begin{bmatrix}0\\0\\0\\0\end{bmatrix}. \tag{7}$$

A non-trivial solution (for ω) of Eq. (7) is obtained by numerical evaluation of the roots of $\mathrm{Det}(\mathbf{Z})=0$. This equation has infinite roots in ω. Substitution of Eq. (6) into Eq. (4) yields

$$Y(X,T)=\sum_{n=1}^{4}A_ne^{z_nX}e^{i\omega T}=\sum_{n=1}^{4}A_n\underbrace{e^{\mathrm{Re}[z_n]X}}_{\text{(i)}}\underbrace{e^{i(\mathrm{Im}[z_n]X+\mathrm{Re}[\omega]T)}}_{\text{(ii)}}\underbrace{e^{-\mathrm{Im}[\omega]T}}_{\text{(iii)}}. \tag{8}$$

It can be seen that $Y(X,T)$ is a product of three exponential terms of which the first term is bounded (since X is bounded), and the second term is periodic since the exponent is imaginary. The third term can grow unbounded with time if $\mathrm{Im}[\omega]<0$ and this represents the onset of flutter instability. The mode and velocity at which the pipe becomes unstable depends on the fluid mass fractions β_i and β_e. The coefficients A_n, $n=1,2,3,4$, can be computed from the nullspace of the matrix $\mathbf{Z}$ in Eq. (7), once ω and z_n, $n=1,2,3,4$, have been determined. These coefficients are needed to estimate the force exerted by the fluid-conveying tube on the surrounding fluid.

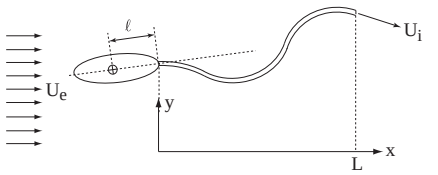

Fig. 3. The proposed submersible, comprises a rigid body and a fluid-conveying flexible tail.

2.2. Slender-body swimming

Fish-like propulsion has been a topic of interest in the academic community for more than 60 years and several robotic platforms have been built (see Triantafyllou et al., 2000; Mcmasters et al., 2008) to exploit the phenomenon. In this paper, we propose a mechanism (see Fig. 3) in which a fluttering fluid-conveying tail provides thrust by both jet and tail action; the tail has the cross-sectional profile of a finned tube like the one shown in Fig. 2. A similar mechanism was constructed in the 1970s (Païdoussis, 1976) and was found to produce positive thrust only if the phase velocity of the tail displacement was greater than the forward speed of the vessel.

Thrust production via a high phase velocity traveling wave was described first in a paper by Lighthill (1960), which used slender-body analysis to approximate the thrust produced by an idealized fish. Lighthill found that a traveling waveform, for example $y(x,t)=f(x)\cos(kx+\Omega t)$, can produce positive thrust if $(\Omega/k)>U_e$, where U_e is the speed of the body relative to the external fluid. The quantity Ω/k is known as the phase velocity. The following equation is the dimensional form of Eq. (8) for a single waveform

$$y_n(x,t)=A_n e^{\mathrm{Re}[Z_n]x}e^{i(\mathrm{Im}[Z_n]x+\mathrm{Re}[\Omega]t)}e^{-i\mathrm{Im}[\Omega]t}, \tag{9}$$

where Z_n and Ω are the dimensional wavenumber and frequency. The waveform described by Eq. (9) will result in positive thrust if

$$\frac{\mathrm{Re}[\Omega]}{\mathrm{Im}[Z_n]}>U_e.$$

The above equation can be non-dimensionalized to the form

$$\frac{\mathrm{Re}[\omega]}{L^2}\left(\frac{EI}{m+M+M_e}\right)^{1/2}\frac{L}{\mathrm{Im}[z_n]}>u_e\left(\frac{EI}{M_e}\right)^{1/2}\frac{1}{L}\Rightarrow\frac{\mathrm{Re}[\omega]}{\mathrm{Im}[z_n]}>\frac{u_e}{\beta^{1/2}}. \tag{10}$$

Eq. (10) gives us a condition under which a waveform will generate positive thrust, where $\mathrm{Re}[\omega]/\mathrm{Im}[z_n]$ is the non-dimensional phase velocity of the waveform.

The icthyoid propulsor (Païdoussis, 1976) was described to have a single phase velocity, which was measured by direct observation. While a single phase velocity is relatively simple to determine experimentally, determination of positive thrust is not straightforward in the context of Eq. (8) since it has four traveling waveforms of different, spatially variable amplitudes and phase velocities. In the context of Eq. (8), it is easier to estimate thrust by the method laid out by Lighthill (1960) and Wu (1971). In those papers, a slender[2] fish is considered and the time-averaged thrust $\overline{\tau}$ is given by the relation

$$\overline{\tau}=\tfrac{1}{2}M_e\left[\overline{[\dot{y}^2-(U_e y')^2]}_{x=L}-\overline{[\dot{y}^2-(U_e y')^2]}_{x=0}\right], \tag{11}$$

where $y=y(x,t)$ denotes the displacement of the slender body from its neutral position, $\dot{y}$ and y' denote partial derivatives of y with respect to time and x, and overbar refers to a long-term time average. In the above equation, increasing M_e increases the thrust generated; this leads to the design choice of the finned-tube in Fig. 2. The form of Eq. (11) also makes it clear that a higher forward speed U_e requires a higher velocity $\dot{y}$ to sustain it. Both Lighthill (1960) and Wu (1971) derived the expression in Eq. (11) without the assumption of harmonic motion. If harmonic motion is assumed, the time average over a single cycle is sufficient. Note that Eq. (11) differs slightly from that found in Wu (1971).[3] Wu's assumption that no mass is affected at $x=0$ is relaxed, since we are dealing with a uniform tail rather than a tapered fish which has zero area at the tip.

A similar expression (Lighthill, 1960) was derived for the average power $\overline{P}$ required to provide the displacements $y(x,t)$

$$\overline{P}=U_e M_e\left[\overline{[\dot{y}(\dot{y}+U_e y')]}_{x=L}-\overline{[\dot{y}(\dot{y}+U_e y')]}_{x=0}\right], \tag{12}$$

which includes the power lost in the vortex wake. Eqs. (11) and (12) indicate that a large magnitude of $\dot{y}$ produces greater thrust but also requires higher energy input. This can also be verified from the expression of the Froude efficiency

[2] A definition of "slender body" can be found in Section 2 of Wu (1971).
[3] Eq. (47) in that work.

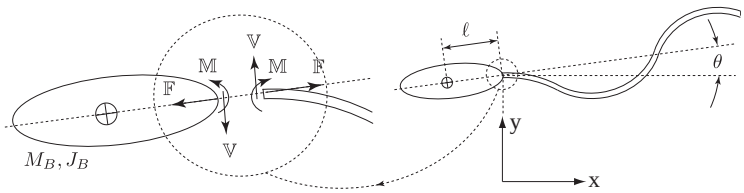

Fig. 4. Free-body diagrams of the rigid body and tail of the submersible in Fig. 3.

(Lighthill, 1960) of the motion of the slender body

$$\eta = \frac{\overline{\tau} U_e}{\overline{P}}. \tag{13}$$

In this paper we consider a submersible which comprises a rigid body and a fluid-conveying tail. The expression for efficiency in Eq. (13) does not account for power lost to internal fluid shearing in the pipe, or external drag. The actual efficiency of the submersible will therefore be somewhat lower after these effects are accounted for.

3. Fluid-conveying pipe affixed to a rigid body

3.1. Simplified boundary conditions

The complete dynamics of a submersible with a fluid-conveying fluttering tail, as shown in Fig. 3, was derived by Hellum et al. (2010a). However, a simplified model that permits better understanding of the important parameters governing the motion is desirable. To this end, we make the following assumptions:

(i) The rigid body is symmetric about the plane containing the neutral surface of the undeformed beam.
(ii) The rotation of the rigid body, denoted by θ in Fig. 4, is small. This is in addition to the Euler–Bernoulli beam assumption that the slope of the tail is small everywhere along its length.
(iii) The submersible has zero acceleration in the x direction. This allows us to ignore the "forces" that arise from a non-inertial reference frame.
(iv) The added mass coefficient associated with the rigid body is zero. This assumption simplifies the analysis by allowing us to concentrate on the geometry of the rigid body in the xy plane. This is equivalent to the assumption that the rigid body is a planar lamina in the xy plane.

The above assumptions allow us to write the boundary conditions for the fluid-conveying tail[4] at $x=0$ as follows:

$$\left[EI\frac{\partial^3 y}{\partial x^3} + M_B\left(\frac{\partial^2 y}{\partial t^2} - \ell\frac{\partial^3 y}{\partial x \partial t^2}\right)\right]_{x=0} = 0, \tag{14a}$$

$$\left[EI\frac{\partial^2 y}{\partial x^2} - (J_B + M_B\ell^2)\frac{\partial^3 y}{\partial x \partial t^2} + M_B\ell\frac{\partial^2 y}{\partial t^2}\right]_{x=0} = 0, \tag{14b}$$

where M_B is the mass of the rigid body, and J_B is the mass moment of inertia of the rigid body about its center of mass, and ℓ is the distance of the center of mass of the rigid body from the base of the tail. The boundary conditions in Eq. (14) can be derived from the free-body diagram of the rigid body in Fig. 4 as follows:

$$-\mathbb{V} = M_B\left[\frac{\partial^2 y}{\partial t^2} - \ell\frac{\partial^3 y}{\partial x \partial t^2}\right]_{x=0}, \quad \mathbb{M} - \ell\mathbb{V} = J_B\left[\frac{\partial^3 y}{\partial x \partial t^2}\right]_{x=0}.$$

It should be pointed out that the variable θ in Fig. 4 denotes the orientation of the rigid body, which is equal to the slope of the tail at $x=0$, *i.e.*, $\theta = [\partial y/\partial x]_{x=0}$. Since the rigid body is symmetric about the plane containing the neutral surface of the undeformed beam, the force $\mathbb{F}$ does not affect the boundary conditions.

Using Eq. (2), we can obtain the non-dimensional form of Eq. (14a):

$$\left[Y''' + \mu(\ddot{Y} - \lambda\ddot{Y}')\right]_{X=0} = 0, \tag{15a}$$

$$\left[Y'' - \mu\{(\psi_B + \lambda^2)\ddot{Y}' - \lambda\ddot{Y}\}\right]_{X=0} = 0, \tag{15b}$$

[4] The result given here is similar to that in Bhat and Wagner (1976) with the exception that they have been derived here at $x=0$ rather than $x=L$.

where

$$\mu = \frac{M_B}{(m+M+M_e)L}, \quad \lambda = \frac{\ell}{L}, \quad \psi_B = \frac{J_B}{M_B L^2}$$

are non-dimensional parameters of the rigid body. Physically, μ is the ratio of its mass to the mass of the rest of the system, λ is a non-dimensional distance, and ψ_B is the square of the non-dimensional radius of gyration. Note that Eq. (15a) provides the boundary conditions for a free end as $\mu \to 0$, and that of a clamped end as $\mu \to \infty$. The free-end conditions can be shown easily whereas the clamped-end conditions can be shown by allowing μ to approach ∞ in Eqs. (15a) and (15b) which yields

$$[\ddot{Y} - \lambda \ddot{Y}']_{X=0} = 0, \tag{16a}$$

$$[(\psi_B + \lambda^2)\ddot{Y}' - \lambda \ddot{Y}]_{X=0} = 0. \tag{16b}$$

Since $\psi_B \neq 0$, it can be readily shown from Eqs. (16a) and (16b) that $\ddot{Y} = \ddot{Y}' = 0$ at $X=0$. Assuming zero initial velocities, *i.e.*, $\dot{Y}(0,0) = \dot{Y}'(0,0) = 0$, we obtain the clamped end conditions $\dot{Y}(0,T) = \dot{Y}'(0,T) = 0$.

3.2. Method of analysis

The simplified boundary conditions for a fluid-conveying pipe affixed to a rigid body are investigated in the same manner as that of a cantilever pipe, which was discussed in Section 2.1. Using the boundary conditions in Eqs. (15a) and (15b) we get the following relation that is similar to Eq. (7):

$$\begin{bmatrix} \eta_1 & \eta_2 & \eta_3 & \eta_4 \\ \zeta_1 & \zeta_2 & \zeta_3 & \zeta_4 \\ z_1^2 e^{z_1} & z_2^2 e^{z_2} & z_3^2 e^{z_3} & z_4^2 e^{z_4} \\ z_1^3 e^{z_1} & z_2^3 e^{z_2} & z_3^3 e^{z_3} & z_4^3 e^{z_4} \end{bmatrix} \begin{bmatrix} A_1 \\ A_2 \\ A_3 \\ A_4 \end{bmatrix} = \begin{bmatrix} 0 \\ 0 \\ 0 \\ 0 \end{bmatrix}, \tag{17}$$

where η_n, ζ_n, $n=$ 1,2,3,4, are defined by the relations

$$\eta_n = z_n^2 + \mu\omega^2[(\psi_B + \lambda^2)z_n - \lambda],$$

$$\zeta_n = z_n^3 - \mu\omega^2(1 - \lambda z_n).$$

Eq. (17) leads to a solution of the form given by Eq. (8). Since the proposed application of the swimming submersible requires the oscillations of the fluttering tail not to grow with time, the points of neutral stability, *i.e.*, $\mathrm{Im}[\omega] = 0$, are sought in the u_i–u_e space.

For a given μ, λ, ψ_B, β_i, β_e, and a given forward velocity u_e, the value of u_i for which $\mathrm{Im}[\omega] = 0$ can be found through the analysis of an Argand diagram, an example of which is provided in Fig. 5. This diagram is constructed (Hellum et al., 2010b; Gregory and Païdoussis, 1966) by determining the natural frequencies of a set of modes at $u_i = 0$, then gradually incrementing u_i to determine $\mathrm{Re}[\omega]$ and $\mathrm{Im}[\omega]$ for higher values of u_i. The natural frequencies at the onset of flutter instability, ω_{cr}, are the locations where the resultant curves cross the imaginary axis. The velocities at which this occurs are referred to as critical velocities, u_{cr}. This procedure yields a single neutrally stable point in the u_i–u_e space. Clearly, while it is possible to search the entire u_i–u_e space for these neutrally stable points, this would require construction of a large number of Argand diagrams to obtain an acceptable resolution in u_e, which is prohibitively time-expensive. To mitigate this problem, an automated method similar in character to that discussed above is proposed.

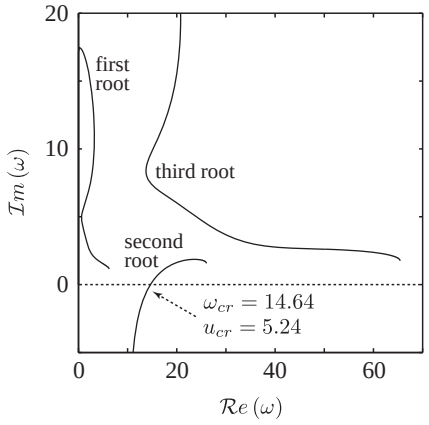

Fig. 5. Argand diagram for the first three modes of oscillation for $\beta_i = 0.01$, $\beta_e = 0.9$, $\lambda = 1/2$, $\psi_B = 1/12$, $\mu = 2.25$ and $u_e = 1.0$.

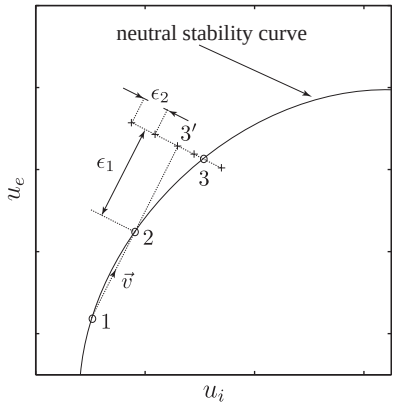

Fig. 6. Figure illustrating the procedure used to find the neutral stability curve.

In the automated method, the value of u_i required for neutral stability at $u_e = 0$ is first computed by interpolating values of u_i for which $Im[\omega] \approx 0$. This is repeated once more for $u_e = \epsilon$, where ϵ is a small number. Subsequent points may be found in the following manner, which is explained with the help of Fig. 6. For a set of two consecutive neutrally stable points already determined, such as the points marked 1 and 2 in Fig. 6, the next point is guessed to exist at point 3′ at a distance ϵ_1 from point 2 along the vector $\vec{v}$ drawn from point 1 to point 2. Several points at which to compute ω are then chosen near point 3′ along a vector perpendicular to $\vec{v}$. These points are separated from each other by the distance ϵ_2. The value for ω_{cr} may now be found by interpolation, and computation of the critical values of u_i and u_e follows trivially. This procedure, in which the direction of iteration is nearly perpendicular to the curve, was necessary to navigate some of the sharp turns in the neutral stability curves given in the next section. In general, lower values of ϵ_1 and ϵ_2 are needed for curves with sharper turns, and in the current work, $\epsilon_1 = 0.02$, $\epsilon_2 = 0.002$ were found to suffice. The method was found to be robust as well; while we present results for a single rigid body of variable mass in this paper, changes in other parameters can be easily accommodated.

4. Stability, thrust and efficiency

4.1. Neutral stability

We obtained neutral stability curves in the u_i–u_e space for a fluid-conveying pipe affixed to a rigid body, using the simplified boundary conditions discussed in Section 3. These neutral stability curves were obtained for various values of μ. The values of the other parameters were chosen as follows:

$$\beta_i = 0.01, \quad \beta_e = 0.9, \quad \lambda = 1/2, \quad \psi_B = 1/12.$$

The values of β_i and β_e used here reflect the finned-tube geometry, shown in Fig. 2. The nature of this geometry is such that a large amount of external fluid is associated with the oscillations of the tail and this explains the relatively large value of β_e. Likewise, the small value of β_i reflects the small area through which internal fluid is conveyed. The values of λ and ψ_B correspond to a uniform cylinder with length equal to that of the tail.

The neutral stability curves are shown in Fig. 7. The area inside each curve (towards the origin) represents the region where the tail does not flutter whereas the area outside represents the region where the tail flutters. The difference between the low-μ and high-μ curves is striking. For values of $u_e < 2.9$, the value of u_i required to create flutter decreases with increase in the value of μ. The confluence of all the curves at $u_e \approx 2.9$ is also interesting though no theoretical reason for this confluence is apparent. It should be mentioned that the curves' tendency to pass close to one another is not a unique scenario. Recall that the rigid body can be described by the parameters ψ_J, λ, and μ, of which we have only investigated the latter in detail in this work. Changing the values of ψ_J and λ does not, in our experience, remove this tendency of the curves to intersect at a point, though the point in u_i–u_e space is different.

For values of $u_e > 2.9$, higher values of μ are neutrally stable at a higher value of u_e for a given value of u_i. This implies that for a given flow rate provided by the prime mover, a tail affixed to a hull of larger mass will tend to flutter at higher forward speed. The curves also indicate that higher values of μ are neutrally stable at a higher value of u_i for a given value of u_e. This implies that for a given external flow, a tail affixed to a hull of larger mass will require higher internal flow to flutter.

Fig. 8 plots the relationship between u_e and ω_{cr}. It can be seen from this figure that for high mass ratios, there exist certain regions of the u_e parameter space where ω_{cr} is sensitive to u_e. This sensitivity may be used to determine a "sweet spot", where a higher oscillation frequency may be obtained with a minimal change in u_e. This increase in oscillation frequency and concomitant increase in $\dot{y}$ will increase the thrust produced by the beam, per Eq. (11), and can be used for designing high-acceleration maneuvers for the submersible. Thrust production and efficiency in the context of Eqs. (11) and (12) are discussed in the next two sections.

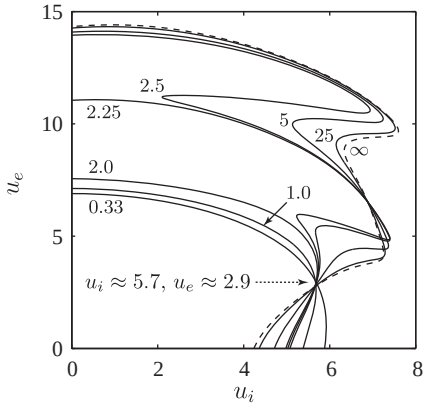

Fig. 7. Neutral stability curves for different values of μ.

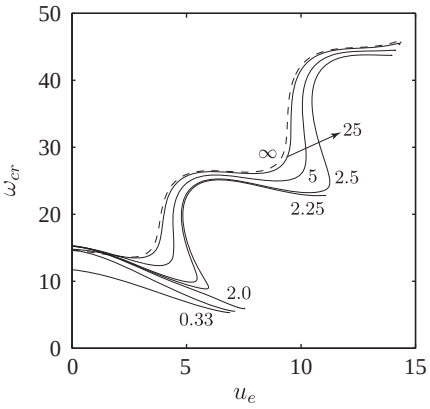

Fig. 8. Plot showing the relationship between ω_{cr} and u_e for different values of μ.

4.2. Thrust characteristics

To determine the thrust produced by the fluttering tail of the proposed submersible, we non-dimensionalize Eq. (11) and compute the average over one cycle as follows:

$$\tau^* = \frac{\overline{\tau} L^2}{EI} = \frac{\omega_{cr}}{4\pi} \int_0^{2\pi/\omega_{cr}} \left\{ [\beta_e \dot{Y}^2 - u_e^2 Y'^2]_{X=1} - [\beta_e \dot{Y}^2 - u_e^2 Y'^2]_{X=0} \right\} dT. \tag{18}$$

The function $Y(X,T)$ is found by the method laid out in Section 2.1, and takes the form of Eq. (8). Eq. (8) has both real and imaginary parts; only the real part is physically manifest and contributes to the thrust. Assuming neutral stability ($\mathrm{Im}[\omega] = 0$), the real part of Eq. (8) is

$$Y(X,T) = \sum_{n=1}^{4} e^{\mathrm{Re}[z_n]X} \left\{ \mathrm{Re}[A_n] \cos(\mathrm{Im}[z_n]X + \mathrm{Re}[\omega]T) - \mathrm{Im}[A_n] \sin(\mathrm{Im}[z_n]X + \mathrm{Re}[\omega]T) \right\}. \tag{19}$$

The coefficients A_n in Eq. (19) are found by computing the nullspace of the matrix in Eq. (17). The terms $\dot{Y}$ and Y' in Eq. (18) can then be obtained from Eq. (19) through differentiation.

Fig. 9 reproduces the curves of neutral stability in Fig. 7 with dark lines depicting the region on each curve where the thrust is negative. Notice that no value of μ allows thrust-producing flutter instability at $u_i = 0$. This matches with our physical intuition that a flapping flag cannot generate thrust. At low values of u_i, the positive hydrodynamic work is predominantly contributed by the external fluid and reduces the energy of that fluid; this phenomenon can be put to use in power generation (Tang et al., 2009). It is also interesting to note that systems with lower values of μ can produce thrust at lower values of u_i than systems with higher values of μ, though the high-μ systems have higher forward speed u_e.

It is important to remember, however, that merely having positive thrust from the tail does not guarantee that a given u_i–u_e point can be reached. The system's drag and the thrust of the fluid jet will also govern the submersible's top speed. Since the drag of the system will, for a neutrally buoyant vessel, be strongly related to the displacement and mass, we will reserve these concerns for a later work more closely tied to the physical realization of the submersible.

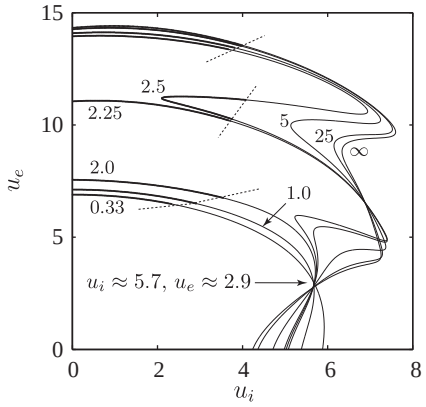

Fig. 9. The darkened region of each neutral stability curve (left of the dotted lines) depicts the region of negative thrust.

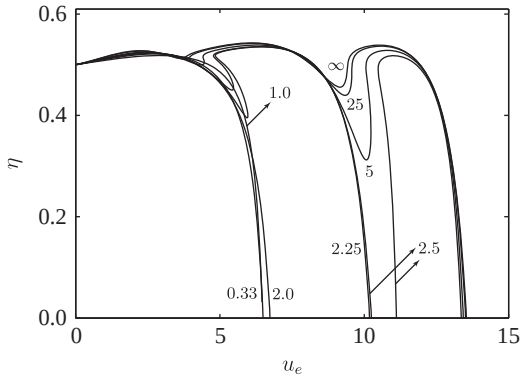

Fig. 10. Efficiency for neutrally stable points in the u_i–u_e space and for different values of μ. Note that the curve for $\mu = 2.5$ is unique in that it has an interim region of zero efficiency.

Finally, it should be mentioned that the calculations presented here are purely concerned with the thrust produced by the traveling waveform in the fluttering tail. As such, the thrust produced by the fluid jet is not considered. However, it has been shown through experiments (Païdoussis, 1976) that this loss of thrust can be overcome such that the combined jet and tail action produces a net thrust that is higher than that of a fixed jet.

4.3. Hydrodynamic efficiency

Similar to the expression for thrust, Eq. (12) can be non-dimensionalized and the average over one cycle computed, to give the average non-dimensional power W^*:

$$P^* = \frac{\overline{P} M_e^{1/2} L^3}{(EI)^{3/2}} = \frac{\omega_{cr}}{2\pi} \int_0^{2\pi/\omega_{cr}} \left\{ [\beta_e u_e \dot{Y}^2 - u_e^2 \beta_e^{1/2} Y' \dot{Y}]_{X=1} - [\beta_e u_e \dot{Y}^2 - u_e^2 \beta_e^{1/2} Y' \dot{Y}]_{X=0} \right\} dT. \tag{20}$$

From Eq. (13), the expression for Froude efficiency can be written as

$$\eta = \frac{\overline{\tau} U_e}{\overline{P}} = \frac{\tau^* u_e}{P^*}. \tag{21}$$

Efficiencies computed using Eq. (21) are plotted with respect to u_e for various values of μ in Fig. 10. Each curve plots the efficiency for neutrally stable points in the u_i–u_e space. Per the discussion in Wu (1971), Eq. (21) has meaning only when the thrust is positive, and therefore, Fig. 10 plots the efficiency only for neutrally stable points with positive thrust, the non-darkened regions of Fig. 9.

It is interesting to note that the maximum efficiency is insensitive to the value of μ. This will provide flexibility in submersible design since the mass of the hull can be chosen based on other factors such as power source, drag and buoyancy, rather than hydrodynamic efficiency. For each value of μ, the efficiency remains near its peak value for a wide range of u_e. This trend resembles the efficiency curves for tail-swimming fish which are known to maintain efficiency over a broad range of swimming speeds. Incidentally, this broad peak in efficiency is not characteristic of typical marine propellers, which tend to be most efficient over a narrow range of velocities.

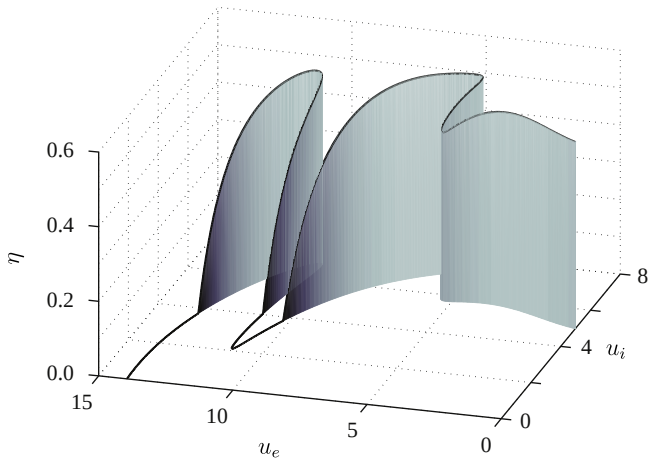

Fig. 11. Efficiency as a function of u_i and u_e for the mass fraction $\mu = 2.5$.

It should be mentioned that the values of efficiency cited here consider only the power used to generate tail motion in the external pressure field and the thrust provided by the tail. Other factors, such as pipe losses and viscous drag, will affect the efficiency of the vehicle when considered as a whole. However, the thrust provided by the fluid jet has also not been considered; a full accounting of the system's efficiency would require further investigation.

A combined perspective in Figs. 9 and 10 is presented in Fig. 11, which depicts the neutral stability curve for $\mu = 2.5$ in three dimensions, with the efficiency shown out of the plane of the page. It is easy to see from this figure that the efficiency of tail motion for a propulsor of this type is dependant on both u_e and u_i. Since a value of zero on the above chart represents a net zero or negative thrust, it should be pointed out that high values of u_e require high values of u_i in order for the tail to oscillate with a thrust-generating waveform.

5. Concluding remarks

The equations of motion for an immersed fluid-conveying pipe affixed to a rigid body have been derived, and the results compared to the classical (Hannoyer and Païdoussis, 1978) case of an immersed fluid-conveying cantilever. It was shown that both the cantilever and free pipe can be expressed as special cases of the rigid body boundary condition. The neutral stability curve in u_i–u_e space was computed over a wide range of values of the rigid body mass fraction μ. The serpentine nature of these curves renders it difficult to make statements about the entire parameter space; nonetheless, some local trends can be observed. At low values of u_e, beams affixed to a rigid body of larger mass become unstable at lower values of u_i, but this trend is reversed for higher values of u_e. It was also found that the stability of the system is insensitive to additional rigid body mass above $\mu = 25$, *i.e.*, the system's behavior is largely indistinguishable from that of a cantilever. This implies that cantilever assumptions would be applicable to large vessels whereas small submersibles require analysis of the type presented in this paper.

Estimates of the sign of the thrust produced by the fluttering tail and the efficiency of that thrust have also been computed. While an estimate regarding the magnitude of the thrust would require consideration of external viscous terms and limit cycle analysis, some general statements about the suitability of this type of propulsor can be made. A relatively high value of u_i is required to drive a thrust-producing flutter instability. Although a system of this type may permit flutter instability for u_i=0, instability driven entirely by the external flow does not provide a thrust-producing motion. This is consistent with our expectation that a flapping flag does not produce thrust. Also, it is clear that smaller values of μ lead to thrust-producing instability at lower values of u_i, though these motions occur at lower forward velocity. We also note that the efficiency of the produced thrust is relatively insensitive to u_e over a wide range of u_e values. Similar observations have been made for live fish (Rohr and Fish, 2006), which move with a waveform *reminiscent* of the traveling waveform generated by a fluid-conveying pipe. It is therefore heartening that one of the great advantages of fish-like propulsion is preserved.

The overall efficiency of the submersible, as opposed to the efficiency of the tail motion, depends on other effects not considered here. These include the efficiency with which the prime mover can generate fluid momentum, pipe losses, and external drag acting on both the hull and the tail. The drag affects the stability of the beam, per (Hannoyer and Païdoussis, 1978), and determines the maximum amplitude of the tail's oscillations. It is important to reiterate here that the relationship between the internal velocity u_i and the submersible's forward speed u_e is determined ultimately by the thrust produced and the vehicle's drag characteristics.

Although we have largely confined our analysis to the single non-dimensional parameter μ, it is possible to investigate the role of many other parameters for a vehicle of this type. Besides the parameters identified in this work, a terminal nozzle might be used at the free end, or a fish-like planform used for the shape of the tail. Analysis of the latter system

must be performed numerically and we expect both tail thrust and efficiency to be improved by such a design. A fish-like planform, with a large reduction in area near the tip of the tail, has been shown (Lighthill, 1970) to be highly efficient for producing thrust on the basis of slender-body theory. A beam with a fish-like planform will be relatively weak at a location near its end, and then much stiffer in that portion which mimics the caudal fin. This should lead to a large, out-of-phase angle between this "fin" and the forward portion of the tail, a condition which is seen in swimming fish.

Acknowledgment

The support provided by the Office of Naval Research, ONR Grant no. N00014-08-1-0460, is gratefully acknowledged.

References

Ashley, H., Haviland, G., 1950. Bending vibrations of a pipeline containing fluid. Journal of Applied Mechanics 17, 229–232.
Bhat, R.B., Wagner, H., 1976. Natural frequencies of a uniform cantilever with slender tip mass in the axial direction. Journal of Sound and Vibration 46 (2), 304–307.
Bourrières, F.-J., 1939. Sur en phenomene d'oscillation auto entrenue en mecanique des fluides reels. Publications Scientifiques et Techniques du Ministére de l'Air 147.
Brennan, C.E., 1982. A review of added mass and fluid inertial forces. Technical Report CR82.010, Naval Civil Engineering Laboratory, Port Hueneme, CA.
Chen, S.S., 1971. Dynamic stability of a tube conveying fluid. ASCE Journal of the Engineering Mechanics Division 97, 1469–1485.
Gray, J., 1936. Studies in animal locomotion VI. The propulsive powers of the dolphin. Journal of Experimental Biology 13, 192–199.
Gregory, R.W., Païdoussis, M.P., 1966. Unstable oscillation of tubular cantilevers conveying fluid. I. Theory. Proceedings of the Royal Society (London) 293, 512–527.
Hannoyer, M.J., Païdoussis, M.P., 1978. Instabilities of tubular beams simultaneously subjected to internal and external axial flows. ASME Journal of Mechanical Design 100, 328–336.
Hellum, A.M., Mukherjee, R., Benard, A., Hull, A.J., 2010a. Dynamic modeling and simulation of a submersible propelled by a fluttering fluid-conveying tail. In: ASME 3rd Joint US-European Fluids Engineering Summer Meeting, Montreal, Canada.
Hellum, A.M., Mukherjee, R., Hull, A.J., 2010b. Dynamics of pipes conveying fluid with non-uniform turbulent and laminar velocity profiles. Journal of Fluids and Structures 26 (5), 804–813.
Lighthill, M.J., 1960. Note on the swimming of slender fish. Journal of Fluid Mechanics 9, 305–317.
Lighthill, M.J., 1970. Aquatic animal propulsion of high hydromechanical efficiency. Journal of Fluid Mechanics 44, 265–301.
Mcmasters, R.L., Grey, C.P., Sollock, J.M., Mukherjee, R., Benard, A., Diaz, A.R., 2008. Comparing the mathematical models of Lighthill to the performance of a biomimetic fish. Bioinspiration & Biomimetics 3, 1–8.
Païdoussis, M.P., 1976. Hydroelastic icthyoid propulsion. AIAA Journal of Hydronautics 10, 30–32.
Païdoussis, M.P., 1978. Marine Propulsion Apparatus. US Patent 4,129,089, December.
Païdoussis, M.P., 1998. Fluid–Structure Interactions: Slender Structures and Axial Flow, vol. 1. Academic Press.
Païdoussis, M.P., 2004. Fluid–Structure Interactions: Slender Structures and Axial Flow, vol. 2. Academic Press.
Païdoussis, M.P., Li, G.X., 1993. Pipes conveying fluid: a model dynamical problem. Journal of Fluids and Structures 7, 137–204.
Rohr, J., Fish, F., 2006. Strouhal number and optimization of swimming by odontocete cetaceans. SSC San Diego Biennial Review, pp. 175–178.
Tang, L., Païdoussis, M.P., Jiang, J., 2009. Cantilevered flexible plates in axial flow: energy transfer and the concept of flutter-mill. Journal of Fluids and Structures 326, 263–276.
Triantafyllou, M.S., Triantafyllou, G.S., Yue, D.K.P., 2000. Hydrodynamics of fishlike swimming. Annual Review of Fluid Mechanics 32, 33–53.
Wu, T.Y.-T., 1971. Hydromechanics of swimming propulsion. Part 1. Swimming and optimum movements of slender fish with side fins. Journal of Fluid Mechanics 46, 545–568.